Orientation effects and figures of merit in advanced 2–2-type composites based on [011]-poled domain-engineered single crystals

Vitaly Yu. Topolov,*[a] Christopher R. Bowen,[b] Andrey V. Krivoruchko,[c] and Ashura N. Isaeva[a]

The paper reports new results that compare the group of performance figures of merit of piezo-active 2–2-type composites based on [011]-poled domain-engineered (1 – x)Pb($Zn_{1/3}Nb_{2/3}$)O_3 – $x$$PbTiO_3$ single crystals, where the main crystallographic axes in the crystal layers are rotated to tailor effective electromechanical properties and related parameters. Examples of the orientation and volume-fraction dependences of the figures of merit are analysed for the first time for the system of 2–2 single crystal / polymer composites and 2–2–0 single crystal / corundum ceramic / polymer composites at x = 0.0475–0.09. The connections between the piezoelectric coefficients d_{3j}^*, energy-harvesting figures of merit $d_{3j}^* g_{3j}^*$ and modified figures of merit $F_{3j}^{*\sigma}$ (j = 1, 2 and 3) are highlighted during rotation of the main X and Y crystallographic axes around the Z axis of the crystal layers. A similar orientation behaviour of d_{3j}^*, $d_{3j}^* g_{3j}^*$ and $F_{3j}^{*\sigma}$ and their large anisotropy are studied at specific volume fractions of the single-crystal component and for a variety of microgeometric architectures of a corundum ceramic / polymer layer with 0–3 connectivity. Maxima of the longitudinal parameters d_{33}^*, $d_{33}^* g_{3j}^*$ and $F_{33}^{*\sigma}$ at x = 0.0475–0.09 and constant volume fraction of the single-crystal component of the 2–2-type composites are observed in a relatively narrow orientation range. A new performance diagram is built to show regions of a large anisotropy of d_{3j}^* and $F_{3j}^{*\sigma}$ in a 2–0–2 composite and, as a result of the large piezoelectric coefficients and figures of merit, the composites show significant potential in the field of piezoelectric energy-harvesting and sensor applications.

Introduction

Piezo-active composites[1-3] based on domain-engineered relaxor-ferroelectric single crystals (SCs), such as (1 – x)Pb($Zn_{1/3}Nb_{2/3}$)O_3 – $x$$PbTiO_3$ (PZN–xPT) or (1 – x)Pb($Mg_{1/3}Nb_{2/3}$)O_3 – $x$$PbTiO_3$ (PMN–xPT) with the perovskite-type structure[4], are of interest for a number of reasons. Firstly, the aforementioned SC components with compositions near the morphotropic phase boundary show outstanding electromechanical properties[5-7] that make them attractive for a variety of piezotechnical, energy-harvesting, hydroacoustic, and transducer applications[1,4]. Secondly, the components strongly influence the piezoelectric performance, electromechanical coupling, hydrostatic and other parameters of composite structures with various connectivity patterns[3,4]. Thirdly, relationships within the fundamental triangle 'composition – structure – property' are yet to be studied in detail for piezo-composites that are based on domain-engineered SCs which are characterised by 1–3, 0–3 or 2–2 connectivity in terms of work by Newnham *et al*.[8] Fourthly, the orientation effects in 1–3 and 2–2 composites[3,9] based on domain-engineered SCs poled in specific crystallographic directions open up new opportunities to improve the hydrostatic piezoelectric response, energy-harvesting figures of merit (FOMs), anisotropy factors, and other parameters of composites. Finally, a system of FOMs[10] introduced for piezoelectric energy harvesters, transducers and related piezotechnical devices has been studied for a group of 1–3 PMN–xPT SC / polymer composites[11] where the main component is a domain-engineered SC poled along the [001] direction of the perovskite unit cell, and the molar concentration x is related to the ferroelectric phase from the 3m symmetry class.

In the past two decades, full sets of electromechanical constants of domain-engineered relaxor-ferroelectric SCs have been determined on samples poled along one of the following perovskite unit-cell directions: [001] (*e.g*. PMN–xPT[12¬14] and PZN–xPT[15,16]), [011] (*e.g*. PMN–xPT[14, 17], PZN–xPT[5¬7], and (1 – x – y)Pb($In_{1/2}Nb_{1/2}$)O_3–yPMN–xPT)[18], or [111] (*e.g*. PMN–xPT[14, 19]). In recent years, progress in the field of relaxor ferroelectrics with a perovskite-type structure has focused on the very high piezoelectric performance of a domain-engineered [001]-poled Sm-doped PMN–0.30PT SC[20], where the molar concentration of Sm is smaller than 0.87%. According to experimental results[20], such a Sm-doped PMN–0.30PT SC is characterised by the longitudinal piezoelectric strain coefficient d_{33} = 3400 – 4000 pC / N and dielectric permittivity $\varepsilon_{33}^{\sigma}/\varepsilon_0 \approx 12000$. The piezoelectric voltage coefficient is evaluated as $g_{33} = d_{33} / \varepsilon_{33}^{\sigma}$ = 32.0 – 37.6 mV·m / N‡. To date, the full set of electromechanical constants of the Sm-doped PMN–0.30PT or related Sm-doped relaxor-ferroelectric SC is yet to published.

In the present paper, we provide the first analysis of the performance and FOMs of a system of 2–2-type composites based on domain-engineered PZN–*x*PT SCs that are poled along the [011] direction of the perovskite unit cell. We note that, for example, the [011]-poled PMN–*x*PT SCs were used as components of parallel-connected 2–2 SC / polymer composites[4] which lead to large hydrostatic parameters of these materials. The aim of our present paper is to demonstrate links between the piezoelectric properties and energy-harvesting parameters of the 2–2-type composites, where a rotation of the main crystallographic axes of the SC component is considered, along with a variation of its volume fraction and microgeometric characteristics in the adjacent layer. Here, the [011]-poled domain-engineered PZN–*x*PT SCs are regarded as the main piezoelectric components of the 2–2-type composites that are examined in the present paper. For the SCs with the composition x = 0.0475–0.09, *i.e.*, near the morphotropic phase boundary[21], full sets of elastic, piezoelectric and dielectric (or electromechanical) constants[5-7] have been measured at room temperature. The aforementioned [011]-poled PZN–*x*PT SCs are characterised by the macroscopic *mm*2 symmetry[5-7], and their piezoelectric charge coefficients d_{3j} obey the condition $d_{31} \neq d_{32} \neq d_{33}$. The work represents the first examination of the performance figures of merit concerned with the 31, 32 and 33 modes of the piezoelectric effect for various orientations of the crystallographic axes of the SC component for 2–2 or related laminar composites based on the [011]-poled domain-engineered SCs. Such data provides information on the design and tailoring of the effective parameters of piezo-composite structures for sensors, energy harvesting and transducer applications.

Model concepts, effective parameters and components of 2–2-type composites

It is assumed that the laminar composite consists of a system of parallel-connected layers of two types, see Fig. 1, and these layers are regularly arranged along the OX_1 axis. The interfaces that separate the layers are parallel to the (X_2OX_3) plane. We consider the layers of two types, where a *Type I* layer represents a domain-engineered SC with a spontaneous polarisation $\boldsymbol{P_s^{(1)}}$, see inset 1 in Fig. 1. The *Type II* layer is either a polymer medium (inset 2 in Fig. 1, a) or a 0–3 ceramic / polymer composite (inset 2 in Fig. 1, b). In the initial position, the main crystallographic axes X, Y and Z of the SC component are oriented as follows: X || OX_1, Y || OX_2 and Z || $\boldsymbol{P_s^{(1)}}$ || OX_3. The same orientation of the main crystallographic axes is written in terms of the perovskite unit-cell direction in the following form: X || [0 $\bar{1}$ 1], Y || [1 0 0] and Z || [0 1 1]. In each Type I layer, a rotation of the main crystallographic axes X, Y around the main crystallographic axis Z || $\boldsymbol{P_s^{(1)}}$ || OX_3 is performed in the (X_1OX_2) plane, and the rotation angle φ is shown in the inset 1 in Fig. 1. Such a rotation mode enables us to maintain a poling axis Z that is parallel to the co-ordinate OX_3 axis for both the Type I layer and composite at various angles φ. The SC / polymer composite is characterised by 2–2 connectivity in terms of Ref. 8.

In the 2–0–2 composite that is also studied here, the *Type II* layer is a ceramic / polymer medium with 0–3 connectivity, see inset 2 in Fig. 1, b. The shape of each ceramic inclusion in the Type II layer (see inset 2 in Fig. 1, b) is spheroidal, so that the equation $(x_1 / a_1)^2 + (x_2 / a_2)^2 + (x_3 / a_3)^2 = 1$ holds for each spheroidal inclusion in the co-ordinate ($X_1X_2X_3$) system. Hereafter $\rho_i = a_1 / a_3 = a_2 / a_3$ is the aspect ratio of the inclusion, and m_i is the volume fraction of the ceramic component in the Type II layer. The semi-axes a_k of each ceramic inclusion are assumed to be much smaller than the thickness of each layer in the composite sample shown in Fig. 1. A regular arrangement of the ceramic inclusions in the polymer matrix obeys the condition that centres of symmetry of these inclusions occupy sites of a simple tetragonal lattice with unit-cell vectors parallel to the co-ordinate OX_f axes.

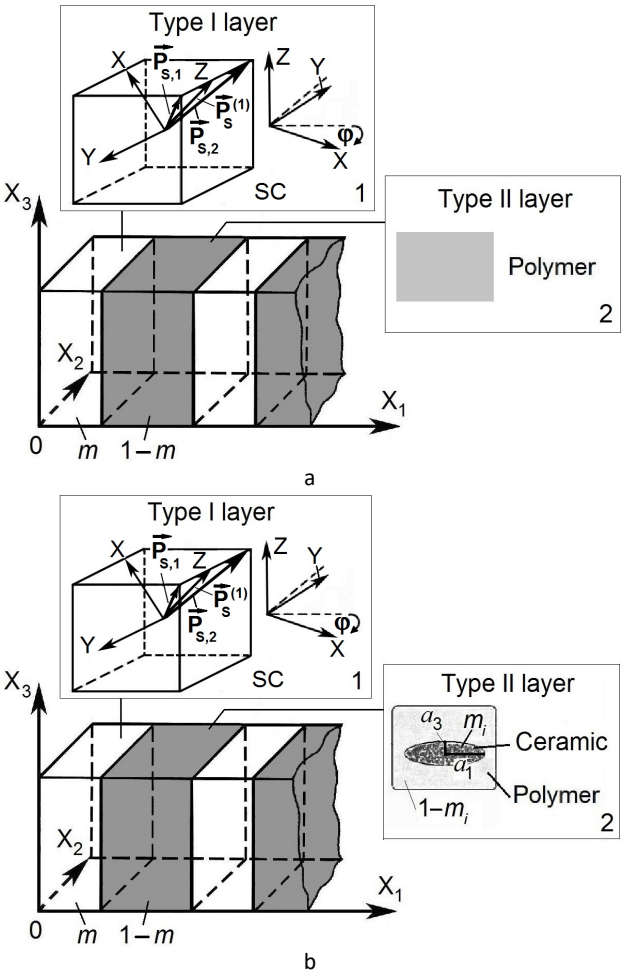

Fig. 1. Schematics of 2–2 (a) and 2–0–2 (b) composites based on domain-engineered SCs. ($X_1X_2X_3$) is the rectangular co-ordinate system. m and 1 – m are volume fractions of the Type I (or SC) and Type II layers, respectively. In inset 1, orientations of domains with spontaneous polarisations $\boldsymbol{P_{s,j}}$ and mode of the rotation of the main crystallographic axes X and Y in the SC component are shown. The Type II layer is either a homogeneous polymer medium (see inset 2 in Fig. 1, a) or a ceramic / polymer medium (see inset 2 in Fig. 1, b).

As is known, the 2–2 relaxor-ferroelectric SC / polymer composites are manufactured by the dice-and-fill method.[22] Wang *et al.*[2] applied the lamination technique to manufacture a 1–3 PMN–0.30PT SC / epoxy composite. Laminated blocks manufactured in work[2] represent a 2–2 composite that becomes a part of the 1–3 composite with planar interfaces between components. The 0–3 ceramic / polymer composite with the

aforementioned regular arrangement of inclusions can be manufactured using solid freeform (or rapid prototyping) method, see Refs. 23, 24. The SC and 0–3 ceramic / polymer layers can be assembled by gluing the layers, as described by Nesterov *et al*.[25] It should be noted that complex assembling procedure was applied to obtain a 2–0–2–0 composite for the first time[25] , and the structure of the 2–0–2–0 composite is more complex than the 2–0–2 composite structure shown in Fig. 1, b.

The effective electromechanical properties of the 2–0–2 composite depend on the rotation angle φ (this angle is related to the Type I layers), the volume fraction m of SC in the composite, and the volume fraction m_i of ceramic and aspect ratio ρ_i of the ceramic inclusion in the Type II layer. The effective properties are evaluated in three stages as follows. The first stage is concerned with evaluation of the full set of elastic compliances $(s_{ab}^{E})'$ at electric field E = const, piezoelectric coefficients d_{ij}' and dielectric permittivities $(\varepsilon_{pr}^{\sigma})'$ at mechanical stress σ = const) of the SC component by taking into account the rotation angle φ shown in the inset 1 of Fig. 1. Formulae[3] are applied to determine the full set of electromechanical constants that are to be considered as tensor values of the following rank: second $[(\varepsilon_{pr}^{\sigma})']$, third $[d_{ij}']$ and fourth $[(s_{ab}^{E})']$. In the present paper we use the matrix (or two-index) form[26] of tensor values that characterise the electromechanical properties of piezoelectric materials.

The second stage of evaluations involves the application of the effective field method[27] to determine the effective properties of the Type II layer, and these properties depend on m_i and ρ_i. In the effective field method, an interaction between the spheroidal inclusions is taken into account[3,27], and the matrix of effective electromechanical properties of the 0–3 composite (Type II layer in the 2–0–2 composite, see inset 2 in Fig. 1, b) is given by

$$|| C^{(0\text{-}3)} || = || C^{(p)} || + m_i (|| C^{(c)} || - || C^{(p)} ||)[|| I || + (1 - m_i)|| S || || C^{(p)} ||^{-1} (|| C^{(c)} || - || C^{(p)} ||)]^{-1}. \quad (1)$$

In Eq. (1) $|| C^{(c)} ||$ and $|| C^{(p)} ||$ are 9 × 9 matrices that characterise the electromechanical properties of ceramic and polymer, respectively, $|| I ||$ is the identity matrix, and $|| S ||$ is the matrix that contains the Eshelby tensor components[28]. Elements of $|| S ||$ from Eq. (1) depend[28] on elements of $|| C^{(p)} ||$ and on the aspect ratio ρ_i of the ceramic inclusion. The effective electromechanical properties of the 0–3 composite are expressed in the general form[3] as follows:

$$|| C^{(0\text{-}3)} || = \begin{pmatrix} || c^{(0-3),E} || & || e^{(0-3)} ||^{t} \\ || e^{(0-3)} || & -|| \varepsilon^{(0-3),\xi} || \end{pmatrix}. \quad (2)$$

The $|| C^{(c)} ||$ and $|| C^{(p)} ||$ matrices from Eq. (1) have the form similar to the form of $|| C^{(0\text{-}3)} ||$ from Eq. (2). In Eq. (2) $|| c^{(0\text{-}3),E} ||$ is the matrix of elastic moduli at E = const, $|| e^{(0\text{-}3)} ||$ is the matrix of piezoelectric coefficients, $|| \varepsilon^{(0\text{-}3),\xi} ||$ is the matrix of dielectric permittivities at mechanical strain ξ = const, and superscript in Eq. (2) is used to denote transposition.

In the third stage, the effective electromechanical properties of the composite are calculated by means of the matrix method[3, 29] that allows for the electromechanical interaction between the composite layers shown in Fig. 1. Hereby the effective properties of the composite can be found from the formula

$$|| C^{*} || = [|| C^{(1)} ||\cdot|| M || m + || C^{(2)} || (1 - m)] [|| M || m + || I || (1 - m)]^{-1}. \quad (3)$$

In Eq. (3) $|| C^{(1)} ||$ and $|| C^{(2)} ||$ are 9 × 9 matrices that describe the electromechanical properties of the Type I and Type II layers, respectively, and $|| M ||$ is used to take into account boundary conditions[3] for electric and mechanical fields at the interface x_1 = const (see Fig. 1). The $|| C^{*} ||$ matrix from Eq. (3) is written in the general form as

$$|| C^{*} || = \begin{pmatrix} || s^{*E} || & || d^{*} ||^{t} \\ || d^{*} || & || \varepsilon^{*\sigma} || \end{pmatrix} \quad (4)$$

Hereafter we use an asterisk (*) to denote the effective properties and parameters of the 2–2-type composite. In Eq. (4) $|| s^{*E} ||$ is the matrix of elastic compliances at E = const, $|| d^{*} ||$ is the matrix of piezoelectric coefficients, and $|| \varepsilon^{*\sigma} ||$ is the 3 × 3 matrix of dielectric permittivities at σ = const. The $|| C^{(1)} ||$ and $|| C^{(2)} ||$ matrices from Eq. (3) have the form similar to that shown in Eq. (4). It should be added that $|| C^{(0\text{-}3)} || \neq || C^{(2)} ||$ as a result of the different sets of electromechanical constants involved in the matrices. A transition from the set of electromechanical constants c_{ab}^{E}, e_{fg} and ε_{pp}^{ξ} to the set of constants s_{kl}^{E}, d_{ij} and $\varepsilon_{qq}^{\sigma}$ is performed using conventional formulae[26] for a piezoelectric medium.

The effective properties of the 2–2 SC / polymer composite depend on the volume fraction of the SC m and on the rotation angle φ. The procedure to evaluate the full set of electromechanical constants of the 2–2 composite contains the first and third stages, and the third stage [see Eq. (3)] is implemented just after the first stage due to the homogeneous polymer medium in the Type II layer, as shown in the inset 2 of Fig. 1, a. The effective properties of the 2–2-type composite are found from Eq. (3) within the framework of the longwave approximation[3], due to the assumption that the thickness of the Type I and Type II layers in Fig. 1 are much smaller than the wavelength of an external field applied to the composite sample.

In the present paper we describe the effect of the rotation of the main crystallographic axes X and Y of the SC component on the effective piezoelectric coefficients d_{3j}^{*} and related FOMs of the 2–2-type composites, where j = 1, 2 and 3. Hereby we highlight links between d_{3j}^{*}, traditional energy-harvesting FOMs

$$(Q_{3j}^{*})^2 = d_{3j}^{*} g_{3j}^{*} \quad (5)$$

and modified FOMs

$$F_{3j}^{*\sigma} = L_{3j}^{*} (Q_{3j}^{*})^2 \quad (6)$$

which are introduced[10] for a piezoelectric stress-driven energy harvester. In Eq. (5) g_{3j}^{*} are piezoelectric voltage coefficients. In Eq. (6)

$$L_{3j}^{*} = [(k_{3j}^{*})^{-1} - ((k_{3j}^{*})^{-2} - 1)^{1/2}]^2 / (k_{3j}^{*})^2 \quad (7)$$

characterise the 'maximum output electrical energy / stored electrical energy' ratio[10] of a piezoelectric material. In Eq. (7)

$$k_{3j}^{*} = d_{3j}^{*} (\varepsilon_{33}^{*\sigma} s_{jj}^{*E})^{-1/2} \quad (8)$$

are electromechanical coupling factors that depend on elements of the $|| C^{*} ||$ matrix from Eqs. (3) and (4). Traditional (or squared) energy-harvesting FOMs $(Q_{3j}^{*})^2$ from Eq. (5) are of value to estimate the 'signal / noise' ratio[3] of a piezoelectric device. The modified FOMs $F_{3j}^{*\sigma}$ from Eq. (6) are used to characterise the effectiveness of a piezoelectric stress-driven harvester[10] in terms of its ability to convert mechanical energy into useable electrical energy.

The components of the studied composites are divided into two groups as follows. The first group comprises of [011]-poled domain-engineered PZN–*x*PT SCs, as shown in Table 1. The simplest orientation of the non-180° domains in the rhombohedral phase under the influence of an electric field ***E*** || [0 1 1], as shown in the inset 1 of Fig. 1, a. At x = 0.07–0.09, *i.e.*, close to the morphotropic phase boundary[21], the heterophase regions of the PZN–*x*PT SC may influence its electromechanical properties to a certain degree. The second group (Table 2) comprises components of the Type II layer, and these components are piezo-passive and isotropic[30-34]. Of specific interest is a corundum ceramic that exhibits very large elastic moduli c_{ab}[30,31] in comparison to c_{ab} of polymers.[19,20] A high-density polyethylene (PE)[33] is considered as the softest component in the studied 2–2-type composites.

The PZN–*x*PT SCs from Table 1 are also of interest as components whose piezoelectric voltage coefficient g_{33} changes in a relatively narrow range. The g_{33} parameter is used to describe a piezoelectric sensitivity[2,3,8] along the poling direction OX_3. For instance, at x = 0.045–0.065, the [011]-poled PZN–*x*PT SCs are characterised[13] by g_{33} from 31.68 to 37.24 mV·m / N. As a comparison, the aforementioned [001]-poled Sm-doped PMN–0.30PT SC[33] outlined in the Introduction is characterised by almost equal g_{33} values, despite the two different d_{33} values. The performance of the [011]-poled PZN–*x*PT SCs makes them attractive to study its influence on the orientation effect, FOM and related parameters of piezo-active composites.

Piezoelectric properties and figures of merit: maxima of parameters and orientation effects

A. 2–2 composites

In the present section we show examples of the volume-fraction (m) and orientation (φ) behaviour of the effective piezoelectric coefficients d_{3j}^* and FOMs $(Q_{3j}^*)^2$ and $F_{3j}^{*\sigma}$ from Eqs. (5) and (6). Our analysis of the orientation dependences of the effective properties of the 2–2-type composites [see the || C^* || matrix from Eq. (3) and Fig. 1] by taking into account the components and its symmetry enables us to state that the effective properties and related parameters Π^* obey the condition

$$\Pi^*(m, \varphi) = \Pi^*(m, 180° - \varphi) \text{ or } \Pi^*(m, \varphi, \rho_i, m_i) = \Pi^*(m, 180° - \varphi, \rho_i, m_i) \quad (9)$$

for the 2–2 or 2–0–2 connectivity, respectively. Due to the validity of Eqs. (9) one can analyse the orientation dependence of the effective properties and parameters of the 2–2-type composites in the range of $0° \le \varphi \le 90°$. The presence of the piezoelectric SC component from the *mm*2 symmetry class in the Type I layer and isotropic piezo-passive components in the Type II layer (see Fig. 1)

Table 1. Elastic compliances s_{ab}^E (in 10^{-12} Pa^{-1}), piezoelectric coefficients d_{ij} (in pC / N) and dielectric permittivities $\varepsilon_{pp}^{\sigma}$ of [011]-poled domain-engineered PZN–*x*PT SCs (macroscopic *mm*2 symmetry) at room temperature

Electromechanical constants	x = 0.0475, Ref. 7	x = 0.055, Ref. 7	x = 0.065, Ref. 7	x = 0.07, Ref. 6	x = 0.09, Ref. 5
s_{11}^E	34.26	39.04	46.99	67.52	73.07
s_{12}^E	–47.45	–56.67	–74.01	–60.16	–63.98
s_{13}^E	26.05	32.65	39.51	3.355	4.256
s_{22}^E	125.35	137.40	170.69	102.0	125.6
s_{23}^E	–74.22	–85.47	–96.76	–54.47	–68.04
s_{33}^E	51.32	60.68	61.47	62.02	67.49
s_{44}^E	14.68	15.46	15.04	15.45	15.12
s_{55}^E	277.78	294.12	333.33	291.5	299.3
s_{66}^E	125.98	155.29	169.08	14.08	16.54
d_{15}	4037	4187	4871	1823	2012
d_{24}	134	207	121	50	118.7
d_{31}	750	858	1191	478	476.0
d_{32}	–1852	–1985	–2618	–1460	–1705
d_{33}	1185	1319	1571	1150	1237
$\varepsilon_{11}^{\sigma} / \varepsilon_0$	8000	8500	9500	8240	8740
$\varepsilon_{22}^{\sigma} / \varepsilon_0$	2600	3050	1500	1865	2075
$\varepsilon_{33}^{\sigma} / \varepsilon_0$	3900	4000	5600	3180	3202

Table 2. Elastic moduli c_{ab} (in 10^{10} Pa) and dielectric permittivity ε_{pp} of isotropic components of the Type II layer of composites at room temperature

Components	c_{11}	c_{12}	$\varepsilon_{pp} / \varepsilon_0$
Corundum ceramic [30,31]	43.6	12.3	10
Polyurethane[32]	0.442	0.260	3.5
Polyethylene[33,34]	0,0778	0,0195	2.3

leads to the relation between the piezoelectric coefficients d_{3j}^* and g_{3j}^* from Eq. (5) as follows:

$$g_{3j}^* = d_{3j}^* / \varepsilon_{33}^{*\sigma}. \quad (10)$$

Based on Eq. (10), we write Eqs. (5) and (6) as

$$(Q_{3j}^*)^2 = (d_{3j}^*)^2 / \varepsilon_{33}^{*\sigma} \quad (11)$$

and

$$F_{3j}^{*\sigma} = L_{3j}^* (d_{3j}^*)^2 / \varepsilon_{33}^{*\sigma}, \quad (12)$$

respectively.

Figure 2 shows typical volume-fraction (m) dependences evaluated for the 2–2 composite. At an angle φ = 49°, absolute maxima of longitudinal FOMs $(Q_{33}^*)^2$ and $F_{33}^{*\sigma}$ are achieved in a specific volume-fraction range. A combination of the piezoelectric and dielectric properties[3] in accordance with Eq. (10) leads to a sharp max g_{33}^* at a volume fraction $m < 0.01$. This is observed at the monotonic dependence of both d_{33}^* (curve 1 in Fig. 2) and $\varepsilon_{33}^{*\sigma}$, see Eq. (11). The non-monotonic behaviour of the piezoelectric coefficient g_{33}^* promotes a non-monotonic behaviour of the FOMs $(Q_{33}^*)^2$ and $F_{33}^{*\sigma}$, see curves 3 and 4 in Fig. 2. Maxima of $(Q_{33}^*)^2$ and $F_{33}^{*\sigma}$ are achieved at larger volume fractions m, however the m values remain small, *i.e.*, they obey the condition $m << 1$. On replacing polyethylene (PE) with polyurethane in the Type II layers, a similar character of the volume-fraction dependences of the piezoelectric properties and FOMs is observed, however the max g_{33}^* becomes smaller and is achieved at a larger volume fraction $m \approx 0.01$. As a consequence, the maxima of FOMs $(Q_{33}^*)^2$ and $F_{33}^{*\sigma}$ are smaller and are achieved at larger volume fractions m. These changes are a result of the presence of polyurethane as a polymer component with a larger stiffness in comparison to PE, as seen by the data in Table 2.

New diagrams in Fig. 3 are built for two groups of the 2–2 composites, namely, PE-containing and polyurethane-containing materials. In these composites at x = 0.0475–0.09, absolute max $[(Q_{33}^*)^2]$ and max $F_{33}^{*\sigma}$ are achieved at rotation angles φ = 48–52° (polyurethane-containing) or φ = 49–56° (PE-containing), and one can observe a correlation between the values and locations of absolute max $[(Q_{33}^*)^2]$ and max $F_{33}^{*\sigma}$. In the polyurethane-containing composites, absolute max $F_{33}^{*\sigma}$ can be found at the volume fraction of SC $m \approx 0.1$, and such volume fractions are reproducible when manufacturing piezo-active 2–2 composites[2]. Data from Fig. 3 suggest that a ratio of absolute max $[(Q_{33}^*)^2]$ and absolute max $F_{33}^{*\sigma}$ undergoes minor changes at variations of the molar concentration x or at changes of the polymer component in the Type II layer. This can be accounted for by minor changes of the L_{33}^* factor from Eq. (12) in the specific φ and m ranges related to the maximum points. Both composites based on the PZN–0.065PT SC demonstrate the best performance, see Fig. 3, and this is due to the large piezoelectric coefficient d_{33}^* as a result of the largest d_{33} value at x = 0.065 in Table 1. It should be noted that the composition with x = 0.065 is located in the vicinity of the morphotropic phase boundary[21] and may have a lower piezoelectric activity in comparison to compositions at x = 0.07 and, in particular, at x = 0.09. In our opinion, the smaller piezoelectric coefficient d_{33} at x = 0.07 and 0.09 (see Table 1) can be achieved in poled SCs[5,6] with specific domain and heterophase structures formed by an external electric field. In addition, defect structures can also lead to smaller d_{33} values in poled SCs. Due to the largest piezoelectric coefficient

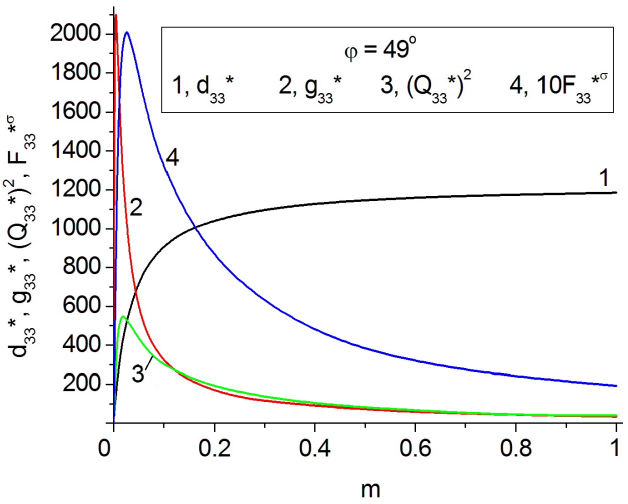

Fig. 2. Volume-fraction (m) dependences of longitudinal piezoelectric coefficients d_{33}^* (in pC / N) and g_{33}^* (in mV·m / N), and FOMs $(Q_{33}^*)^2$ and $F_{33}^{*\sigma}$ (in 10^{-12} Pa^{-1}) of the 2–2 PZN–0.0475PT SC / PE composite at φ = const.

d_{33} at the molar concentration x = 0.065, we place an emphasis on the 2–2-type composites based on the [011]-poled PZN–0.065PT SC.

Examples of the volume-fraction and orientation behaviour of FOMs $(Q_{33}^*)^2$ and $F_{33}^{*\sigma}$ near their absolute maxima are shown for the PZN–0.065PT SC / PE composite in Fig. 4. The graphs in Fig. 4 show that changes in the volume fraction m at the rotation angle φ = const lead to more appreciable changes of $(Q_{33}^*)^2$ and $F_{33}^{*\sigma}$. This is due to the strong influence of the dielectric permittivity $\varepsilon_{33}^{*\sigma}$ on $(Q_{33}^*)^2$ and $F_{33}^{*\sigma}$, see Eqs. (11) and (12). In this context, the volume-fraction range at $m << 1$ is remarkable due to relatively small values of $\varepsilon_{33}^{*\sigma}$ in comparison to the $\varepsilon_{33}^{\sigma}$ of the SC component. The orientation dependence of the piezoelectric properties and FOMs at m = const does not contain sharp extreme points. We note for comparison that the [011]-poled PZN–0.065PT SC in the main crystallographic axes is characterised by FOMs $(Q_{33})^2 = [Q_{33}^*(1, 0°)]^2 = 49.8$ and $F_{33}^{\sigma} = F_{33}^{*\sigma}(1, 0°) = 24.2$ (in 10^{-12} Pa^{-1}). As follows from data in Fig. 4, absolute maxima of FOMs of the PZN–0.065PT-based composite are approximately 12 times $[(Q_{33}^*)^2]$ or ca. 9.2 times $(F_{33}^{*\sigma})$ larger than the aforementioned similar parameters of the SC component at φ = 0°. It can also been seen in Fig. 4 that increasing the volume fraction m to 0.1 enables one to obtain $(Q_{33}^*)^2$ and $F_{33}^{*\sigma}$ values that are approximately five times larger than the similar FOMs of the SC. Such large values of $(Q_{33}^*)^2$ and $F_{33}^{*\sigma}$ are obtained even at deviations from the optimal rotation angles, and are related to the absolute maximum points of $(Q_{33}^*)^2$ and $F_{33}^{*\sigma}$ by a few degrees.

A link between the orientation dependences of the piezoelectric coefficient d_{33}^* and FOMs $(Q_{33}^*)^2 \sim (d_{33}^*)^2$ and $F_{33}^{*\sigma} \sim (d_{33}^*)^2$ [see Eqs. (11) and (12)] is shown in Fig. 5. Here, we use the volume fraction m = 0.1 to characterise the performance of composites and analyse the orientation effects of the system. In Fig. 5 we do not show the orientation dependence of FOMs $(Q_{32}^*)^2$ and $(Q_{31}^*)^2$ due to the simple relation $(Q_{3f}^*)^2 = (Q_{33}^*)^2 (d_{3f}^* / d_{33}^*)^2$ that follows from Eq. (11), where f = 1 and 2. It is important to underline that

(i) local maxima of d_{33}^* (curve 1 in Fig. 5, a), $(Q_{33}^*)^2$ (curve 1 in Fig. 5, b), and $F_{33}^{*\sigma}$ (curve 2 in Fig. 5, b) are observed at an almost equal

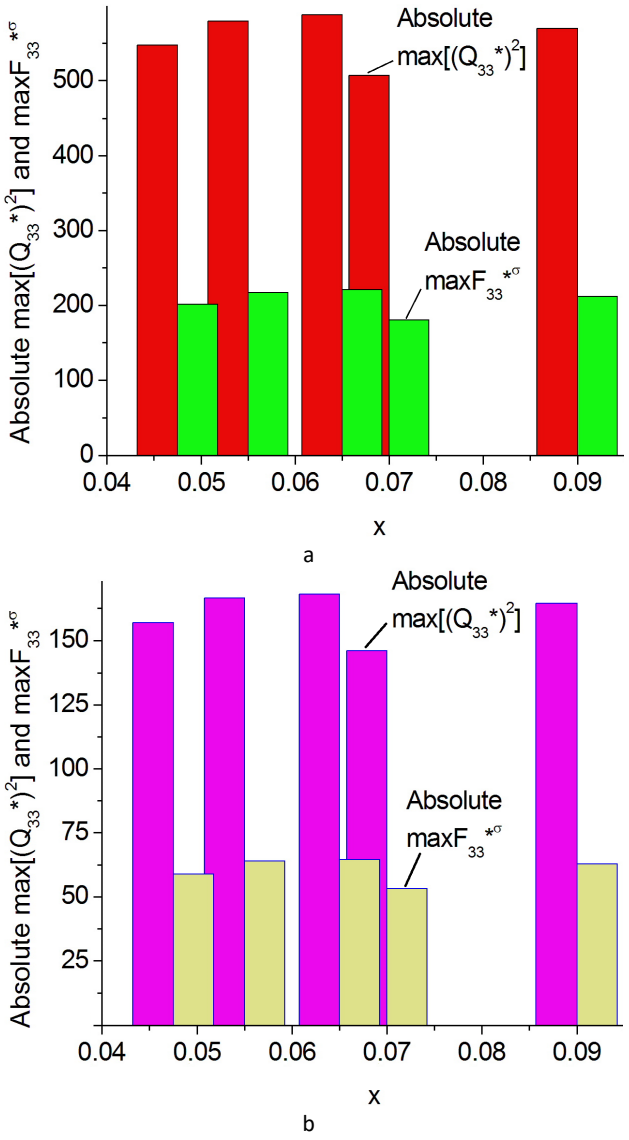

Fig. 3. Absolute maxima of FOMs $(Q_{33}^*)^2$ and $F_{33}^{*\sigma}$ of the 2–2 PZN–*x*PT SC / PE (a) and PZN–*x*PT SC / polyurethane (b) composites at x = 0.0475–0.09.

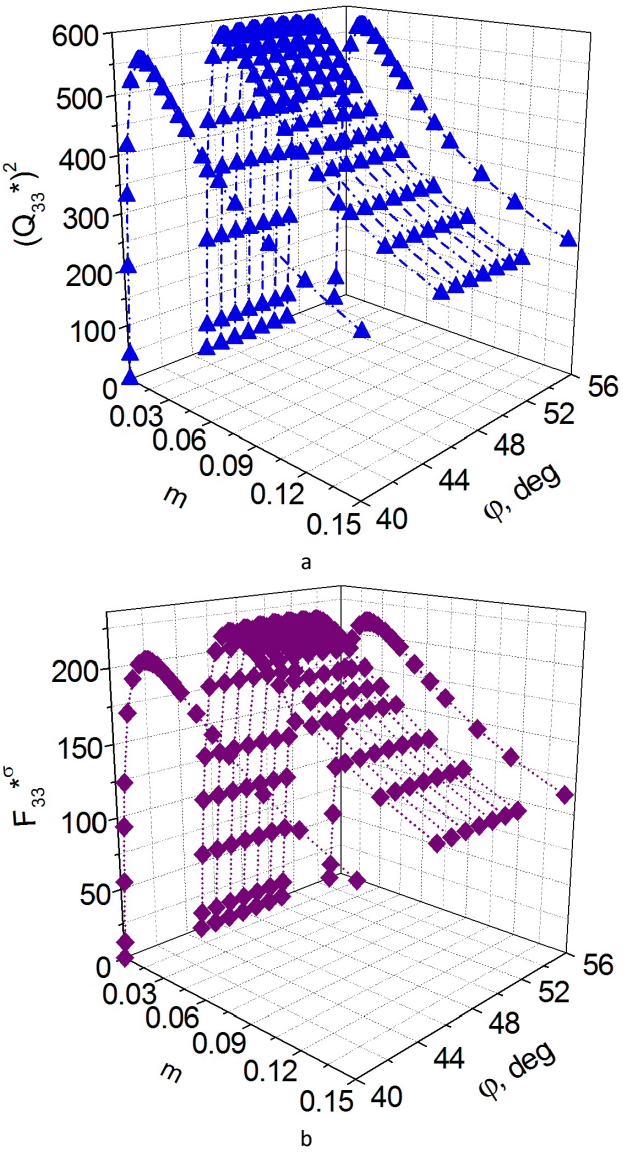

Fig. 4. FOMs $(Q_{33}^*)^2$ (a, in 10^{-12} Pa^{-1}) and $F_{3j}^{*\sigma}$ (b, in 10^{-12} Pa^{-1}) of the 2–2 PZN–0.065PT SC / PE composite in the vicinity of absolute maximum points.

orientation angle φ, this feature is due to the proportionality $(Q_{33}^*)^2 \sim (d_{33}^*)^2$ and $F_{33}^{*\sigma} \sim (Q_{33}^*)^2 \sim (d_{33}^*)^2$ and the limited influence of the the elastic and dielectric properties of the composite on the location of the maximum point of d_{33}^*;

and

(ii) a large anisotropy of FOMs $F_{3j}^{*\sigma}$ is observed close to the local max $F_{33}^{*\sigma}$ due to small values of $F_{31}^{*\sigma}$ and $F_{32}^{*\sigma}$ (curves 2–4 in Fig. 5, b).

The results (i) and (ii) make the studied 2–2 composite attractive for a range of piezotechnical applications, which include sensor elements and elements of energy-harvesting systems. Hereby the 2–2 composite at φ = const becomes polyfunctional due to the system of the studied maxima of effective parameters, including the FOMs. This has no analogs among piezo-active 2–2 composites described in literature.

B. 2–0–2 composites

As seen from Eqs. (9), the effective electromechanical properties and related FOMs of the 2–0–2 composites studied in this work depend on *m*, φ, ρ_i, and m_i , where the aspect ratio ρ_i and volume fraction m_i are related to the corundum inclusions in the Type II layer, see inset 2 in Fig. 1, b. We now examine a variation of the aspect ratio ρ_i and volume fraction m_i, along with the rotation of the main crystallographic axes X and Y in the Type I layer (see the inset 1 in Fig. 1) to show an influence of the Type II layer on the performance of composites. The graphs shown in Figs. 6 and 7 are related to the 2–0–2 PZN–0.065PT-based composite at a volume fraction of SC *m* = 0.1 (see the inset 1 in Fig. 1) to show an influence of the Type II layer on the performance of composites. The graphs shown in Figs. 6 and 7 are related to the 2–0–2 PZN–0.065PT-based composite at a volume fraction of SC *m* = 0.1.

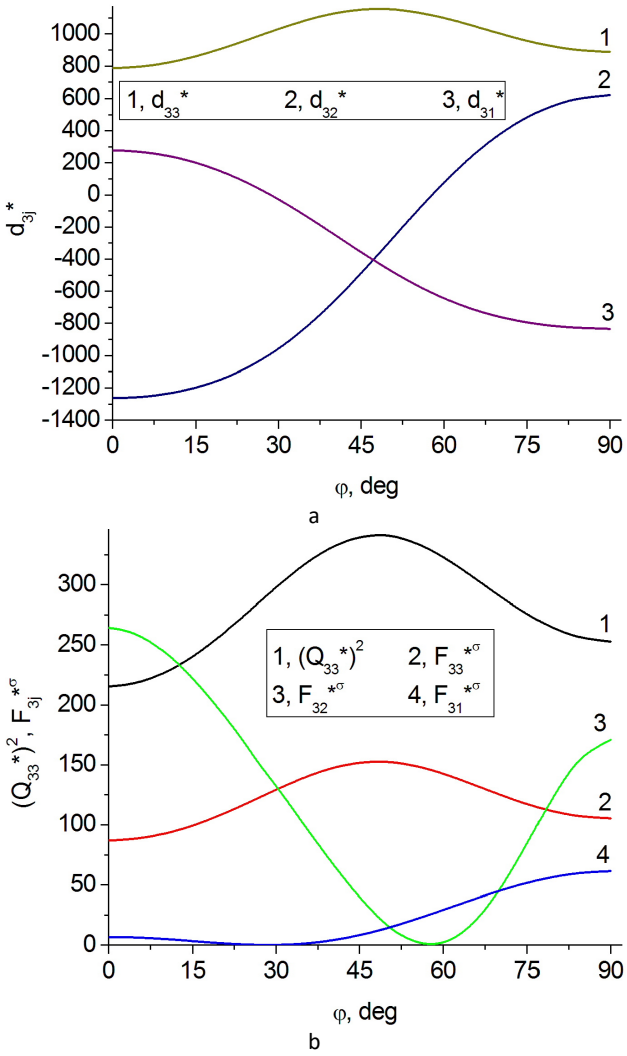

Fig. 5. Orientation (φ) dependences of piezoelectric coefficients d_{3j}^* (a, in pC / N) and FOMs $(Q_{33}^*)^2$ and $F_{3j}^{*\sigma}$ (b, in 10^{-12} Pa^{-1}) of the 2–2 PZN–0.065PT SC / PE composite at the volume fraction of SC m = 0.1.

As in the case of the orientation dependences built for the 2–2 composite in Fig. 5, we observe a strong correlation between maxima of the piezoelectric coefficient d_{33}^* and FOMs $(Q_{33}^*)^2$ and $F_{33}^{*\sigma}$; see, for instance, curves 1 in Fig. 6, a, and 1 and 2 in Fig. 6, b, or curves 1 in Fig. 6, c, and 1 and 2 in Fig. 6, d. In the presence of heavily oblate corundum inclusions, *e.g.* at ρ_i = 100, a significant weakening of the transverse piezoelectric response is observed, and this leads to a considerable decrease of $|\, d_{32}^* \,|$ and $|\, d_{31}^* \,|$ in a wide φ range. We can observe this decrease by comparing curves 2 and 3 in Fig. 6, a to curves 2 and 3 in Fig. 6, c or Fig, 6, e. An increase of the volume fraction m_i of the corundum component in the Type II layer strongly influences its elastic properties. and effective properties of the 2–0–2 composite.

It should be noted that at a volume fraction m_i = 0.2 in the Type II layers, the FOMs $(Q_{33}^*)^2$ and $F_{33}^{*\sigma}$ are still larger than the absolute maxima of these parameters in the 2–2 polyurethane-containing composite, see the diagram in Fig. 3, b. It follows from Fig. 6, b, d and f that a specific shape of the inclusions therein promotes an elastic anisotropy of the Type II layer. Undoubtedly, this influences the effective properties and FOMs of the 2–0–2 composite to a significant extent since the volume fraction of SC m = 0.1 is small in comparison to the volume fraction of the Type II layers, which is determined as 1 – m = 0.9.

A large anisotropy of FOMs $F_{3j}^{*\sigma}$ of the 2–0–2 composite is observed in a relatively wide φ range, and conditions

$$F_{33}^{*\sigma} / F_{31}^{*\sigma} \geq 5 \text{ and } F_{33}^{*\sigma} / F_{32}^{*\sigma} \geq 5 \qquad (13)$$

hold in the vicinity of local maxima of d_{33}^*, $(Q_{33}^*)^2$ and $F_{33}^{*\sigma}$. Increasing the volume fraction m_i of corundum as a high-stiffness component in a polymer medium at $\rho_i >> 1$ promotes the large anisotropy in the FOMs $F_{3j}^{*\sigma}$ of the 2–0–2 composite. With regards to the piezoelectric coefficients d_{3j}^*, they obey the similar conditions for a large anisotropy

$$|\, d_{33}^* / d_{31}^* \,| \geq 5 \text{ and } |\, d_{33}^* / d_{32}^* \,| \geq 5 \qquad (14)$$

hold simultaneously. The validity of conditions (13) is also observed in a narrower φ range (see Fig. 6, a, c and d); however this is in the vicinity of max d_{33}^*. This good performance is related to conditions (13) and (14)§, and is of value for applications where a longitudinal oscillation mode is dominant and any transverse modes are to be suppressed.

When replacing the heavily oblate corundum inclusions with the spherical inclusions at ρ_i = 1 or with the heavily prolate inclusions at ρ_i = 0.1 in the same Type II layers, we observe a decrease in the piezoelectric coefficient d_{33}^*, related FOMs $(Q_{33}^*)^2$ and $F_{33}^{*\sigma}$, and a validity of conditions (13) in a narrower range. The graphs in Fig. 7 show the orientation behaviour of the piezoelectric properties and FOMs of the 2–0–2 composite, where there are less favoured conditions for a large anisotropy of its parameters. The decrease of max $F_{33}^{*\sigma}$ of the composite containing corundum inclusions at ρ_i = 0.1 in comparison to max $F_{33}^{*\sigma}$ of the composite at ρ_i = 1 (see curves 2 in Fig. 7, b and d) is *ca*. 4 times, and this decrease correlates with the decrease of the elastic compliance s_{33} in the Type II layer from 944 to 213 (in 10^{-12} Pa^{-1}), see Table 3. Changes in the elastic properties of the Type II layer (Table 3) are related with a variation of the aspect ratio ρ_i, and volume fraction m_i of the corundum inclusions within the composite. The heavily oblate shape of the inclusions is preferable to provide a large piezoelectric coefficient d_{33}^* and to weaken a transversal response concerned with d_{31}^* and d_{32}^*, which is mainly due to the large s_{33} / s_{11} ratio. The influence of the elastic properties of the Type II layer on the performance of the 2–0–2 composite can be understood at a careful analysis of Eqs. (6)–(8). One can conclude that the FOMs $F_{3j}^{*\sigma}$ depend not only on the piezoelectric coefficients d_{3j}^* (with a variable anisotropy), but also on the L_{3j}^* concerned with elastic compliances s_{jj}^{*E} in accordance with Eqs. (7) and (8). The elastic anisotropy of the Type II layer in the composite at m = 0.1, *i.e.*, at the 90% volume fraction of the Type II layers therein, will play an important role in forming a large anisotropy of the effective piezoelectric, elastic and other properties, and as a consequence, in achieving a large anisotropy of FOMs from Eqs. (11) and (12).

In Fig. 8 we present a new diagram of regions of validity of conditions (13) and (14). This diagram has been built for a 2–0–2 composite where the Type II layer contains 20% of heavily oblate corundum inclusions. The introduction of oblate inclusions promotes a large elastic anisotropy in the Type II layer, see data in Table 3 at ρ_i = 100. In Fig. 8 we show the volume-fraction (m) region

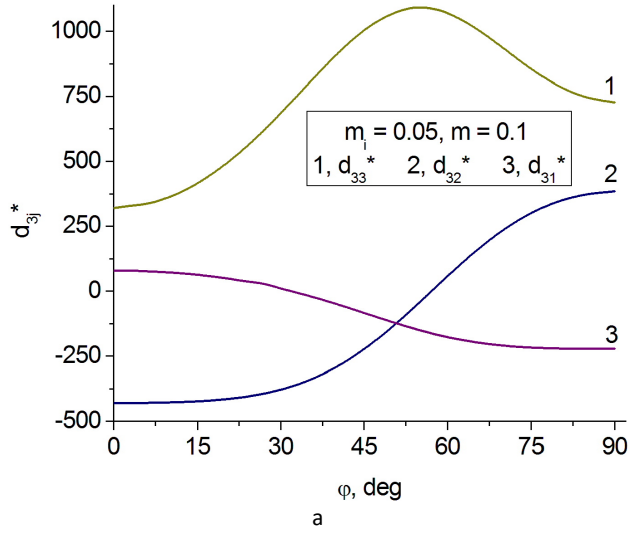

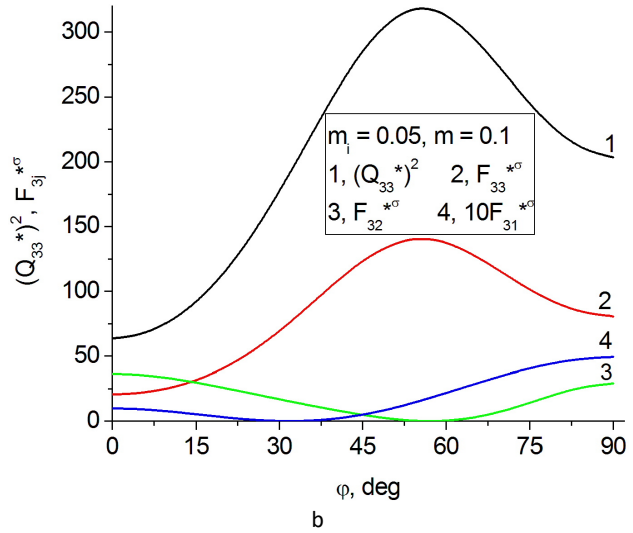

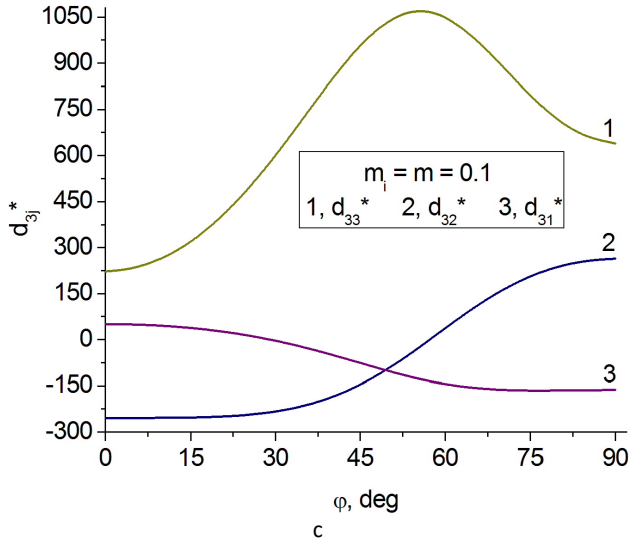

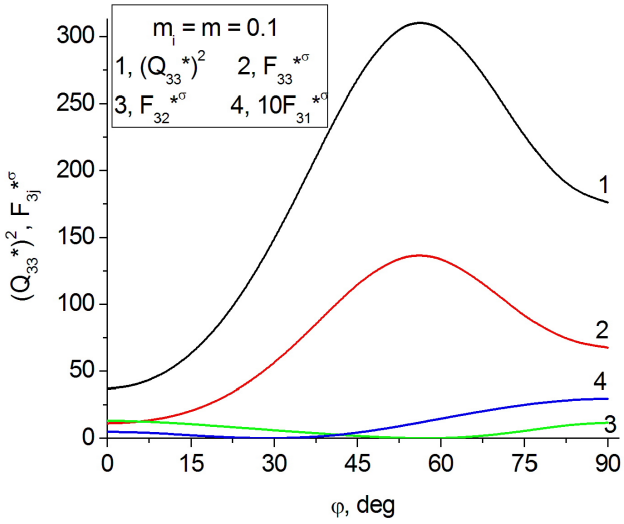

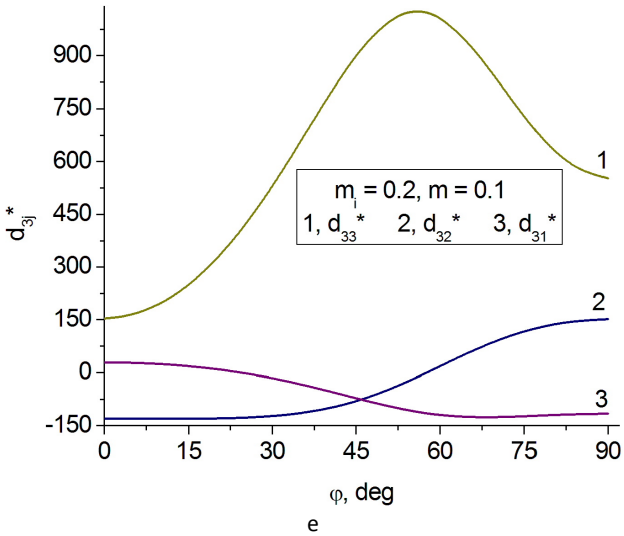

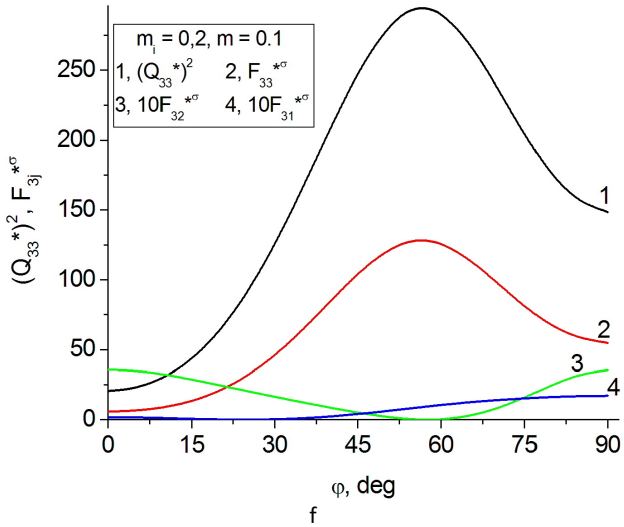

Fig. 6. Orientation (φ) dependences of piezoelectric coefficients d_{3j}^* (a, c and e, in pC / N) and FOMs $(Q_{33}^*)^2$ and $F_{3j}^{*\sigma}$ (b, d and f, in 10^{-12} Pa^{-1}) of the 2–0–2 PZN–0.065PT SC / corundum / PE composite at m = 0.1 and ρ_i = 100. The volume fraction of corundum in the Type II layer is m_i = 0.05 (a and b), 0.1 (c and d), or 0.2 (e and f).

Fig. 6. (continued)

from 0.01 to 0.99, *i.e.*, the almost whole range of volume fractions of SC. In our opinion, a wider φ range of the validity of conditions (13) in comparison to conditions (14) (*cf.* regions 2 and 1 in Fig. 8) can be accounted for by the strong influence of the anisotropic elastic properties of the Type II layer on the effective elastic

properties of the composite and its FOMs $F_{3j}^{*\sigma}$.In a case of the 2–0–2 composite with the same heavily oblate corundum inclusions and polyurethane medium in the Type II layer, we obtain the diagram

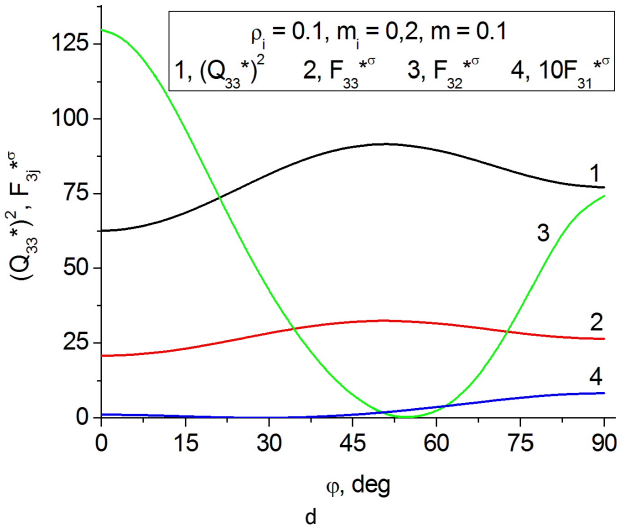

Fig. 7 (continued)

Table 3. Elastic compliances s_{ab} (in 10^{-12} Pa^{-1}) of the corundum ceramic / PE medium (Type II layer in the 2–0–2 composite)

ρ_i	m_i	s_{11}	s_{12}	s_{13}	s_{33}
100	0.05	316	–55.6	–68.5	1260
	0.10	170	–29.5	–38.8	1180
	0.15	113	–19.5	–26.9	1110
	0.20	82.4	–14.2	–20.4	1040
1	0.20	944	–202	–191	944
0.1	0.20	1000	–251	–47.5	213

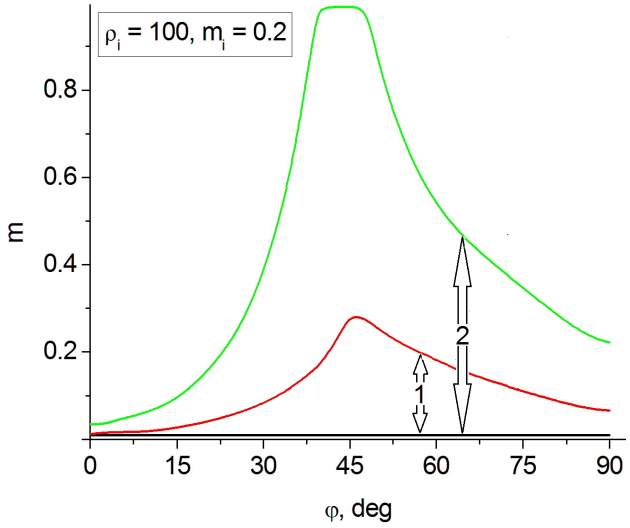

Fig. 8. Diagram that shows the region 1 of validity conditions (14) the region 2 of validity conditions (13) in the 2–0–2 PZN–0.065PT / corundum / PE composite with heavily oblate corundum inclusions (at $\rho_i = 100$) in Type II layers. The volume fraction of corundum in the Type II layer is $m_i = 0.2$.

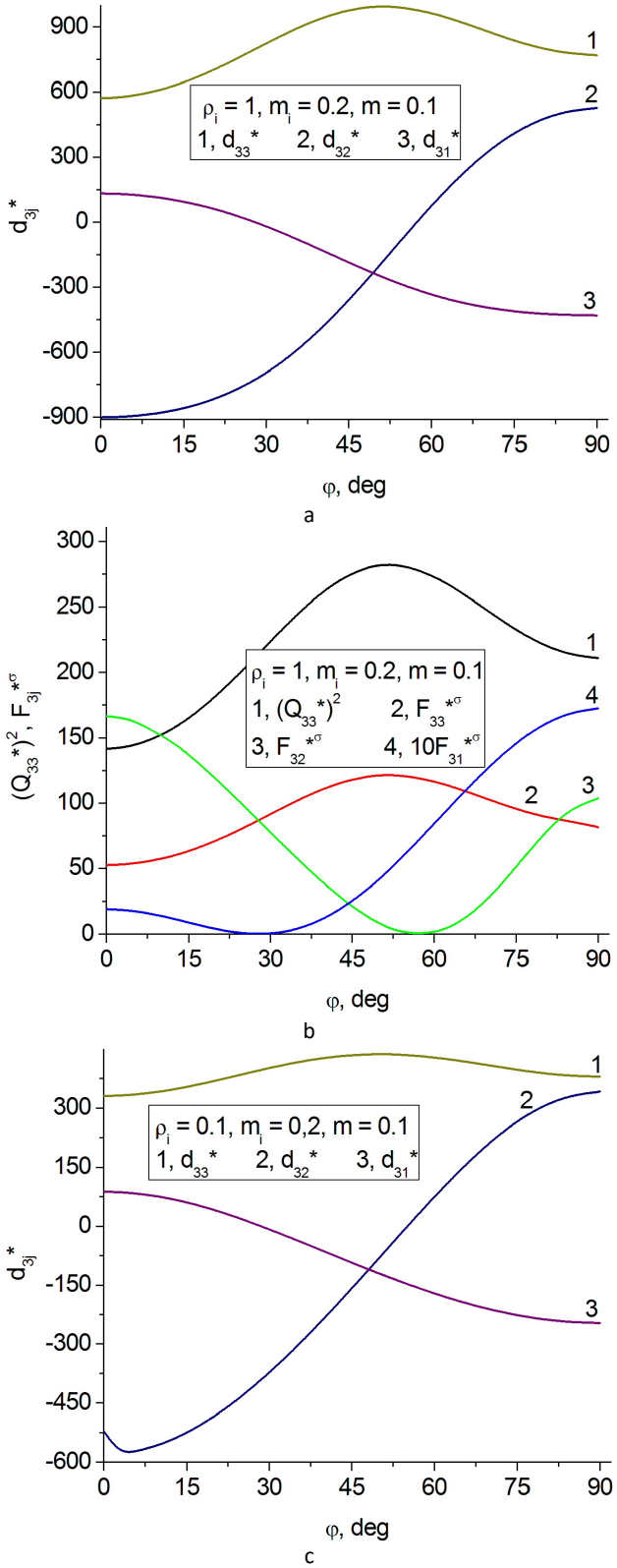

Fig. 7. Orientation (φ) dependences of piezoelectric coefficients d_{3j}^* (a and c, in pC / N) and FOMs $(Q_{33}^*)^2$ and $F_{3j}^{*\sigma}$ (b and d, in 10^{-12} Pa^{-1}) of the 2–0–2 PZN–0.065PT SC / corundum / PE composite at m = 0.1 and ρ_i = 1 (a and b). or ρ_i = 0.1 (c and d).

similar to that shown in Fig. 8. However, the maximal volume fraction m in the region 1 is smaller than 0.2. This is accounted for

by the less pronounced elastic anisotropy of the polyurethane-containing Type II layer. A difference between the elastic properties of corundum and polyurethane decreases in comparison to the difference between the same properties of corundum and PE; see data in Table 2.

Comparison of results

The 2–2-type composites presented here have specific advantages over many piezo-active composites known from literature. For example, max $[(Q_{33}^*)^2]$ and max $F_{33}^{*\sigma}$ of the 2–2 PZN–0.065PT SC / PE at m = 0.1 (see curves 1 and 2 in Fig. 5, b) are larger than $(Q_{33}^*)^2$ and $F_{3j}^{*\sigma}$ of a 1–3 PMN–0.33PT SC / polyurethane[11] at the volume fraction of SC m = 0.05–0.15. In work[11] PMN–0.33PT is the [001]-poled domain-engineered SC component with a piezoelectric coefficient[12] d_{33} = 2820 pC / N, and this d_{33} value is approximately 1.7 times larger than d_{33} = 1571 pC / N of the [011]-poled PZN–0.065PT SC (see Table 1). A lead-free 1–3 composite based on the [001]-poled domain-engineered SC is characterised by FOM $(Q_{33}^*)^2$ = $23.7 \cdot 10^{-12}$ Pa^{-1} at the volume fraction of SC[35] $m \approx 0.52$. The FOMs evaluated for a 1–3 PZT-7A ceramic / araldite composite[36] at a volume fraction of ceramic m_{cer} = 0.2 are $(Q_{33}^*)^2 = 16 \cdot 10^{-12}$ Pa^{-1} and $F_{33}^{*\sigma} = 4.6 \cdot 10^{-12}$ Pa^{-1}. A quasi 1–3 lead-free composite from work[37] is characterised by FOM $(Q_{33}^*)^2 = 18 \cdot 10^{-12}$ Pa^{-1}. As follows from studies on a porous ferroelectric $BaTiO_3$ material[10], its FOM $F_{33}^{*\sigma}$ equals approximately $2 \cdot 10^{-12}$ Pa^{-1}, and the inequality $F_{33}^{*\sigma} / F_{31}^{*\sigma} >> 1$ holds in a wide porosity range, *i.e.*, a large anisotropy of FOMs is achieved. For porous structures obtained using a ferroelectric $BaTIO_3$ ceramic[10], the condition $F_{31}^{*\sigma} = F_{32}^{*\sigma}$ is valid. It should be added that the piezoelectric coefficient d_{33} of a poled monolithic $BaTiO_3$ ceramic[3,10,30] is an order-of-magnitude smaller than d_{33} of the PZN –xPT SCs from Table 1.

A comparison of the performance of the studied 2–2 composite (see Figs. 4 and 5) with the performance of its 2–0–2 analog at the same SC component and its volume fraction m (see Figs. 6 and 7) suggests that the larger anisotropy of FOMs $(Q_{33}^*)^2$ and $F_{33}^{*\sigma}$ can be regarded as an advantage of the 2–0–2 composite even at the smaller $(Q_{33}^*)^2$ and $F_{33}^{*\sigma}$ values.

Conclusions

In this paper new orientation effects have been studied for two systems of 2–2-type composites based on [011]-poled domain-engineered relaxor-ferroelectric PZN–xPT single crystals (SCs) for compositions x = 0.0475–0.09. The effective piezoelectric properties and energy-harvesting performance FOMs depend not only on volume fractions of components, but also on the rotation angle in the SC component and on the aspect ratio of corundum inclusions. Orientation dependences of FOMs from Eqs. (11) and (12) are compared for the 2–2 and 2–0–2 composites.

Large values of longitudinal FOMs $(Q_{33}^*)^2 \sim 10^{-10}$ Pa^{-1} and $F_{33}^{*\sigma} \sim 10^{-10}$ Pa^{-1} are observed for the studied 2–2-type composites. A large anisotropy of their effective parameters [see conditions (13) and (14)] is achieved due to an orientation effect, and in the 2–0–2 composites also due to the appreciable elastic anisotropy of the Type II layer. The orientation effect considered in our study is caused by a rotation of the main crystallographic axes X and Y in the Type I layer (see inset 1 in Fig. 1), and the optimal rotation angle is found in the vicinity of φ = 50°, irrespective of the polymer component in the Type II layer. The remarkable performance of the studied composites correlates with the maxima of the longitudinal piezoelectric coefficient d_{33}^* and related FOMs $(Q_{33}^*)^2$ and $F_{33}^{*\sigma}$. These maxima are observed at the almost equal rotation angle φ (see Figs. 5–7), and this has no analogs among the 2–2-type composites known from literature. The result on maxima of d_{33}^*, $(Q_{33}^*)^2$ and $F_{33}^{*\sigma}$ can lead to the manufacture of advanced 2–2-type composites with specific cuts of SC layers in a specific volume-fraction (m) range.

Of independent interest is the 0–3 corundum ceramic / PE composite medium in the Type II layers of the 2–0–2 composite at an aspect ratio of inclusions $\rho_i >> 1$. Such layers that exhibit an appreciable elastic anisotropy, see Table 3, influence the performance of the composite, its FOMs and the anisotropy to a significant extent. The new diagram in Fig. 8 shows that conditions (13) and (14) for the large anisotropy of the piezoelectric properties and related FOMs are valid in the case of the 2–0–2 composite.

The appreciable anisotropy, large piezoelectric coefficients d_{33}^*, FOMs $(Q_{33}^*)^2$ and $F_{33}^{*\sigma}$ of the novel 2–2-type composites examined in this work make them attractive materials for modern piezoelectric sensors and energy-harvesting systems.

Conflicts of interest

There are no conflicts to declare.

Acknowledgements

Research was financially supported by Southern Federal University, grant No. VnGr-07/2020-04-IM (Ministry of Science and Higher Education of the Russian Federation). The authors are grateful to Prof. Dr. I. A. Parinov and Prof. Dr. A. E. Panich (Southern Federal University, Russia), for their interest in the field of advanced piezo-active composites and their applications.

Notes and references

‡ We note that the longitudinal piezoelectric coefficient g_{33} of the [001]-poled Sm-doped PMN–0.30PT SC is smaller than g_{33} of the [001]-poled PMN–0.33PT or PZN–0.07PT SC. The latter SCs are characterised by the largest piezoelectric coefficient d_{33} among the domain-engineered PMN–xPT or PZN–xPT SCs poled along [001]. Based on experimental values of the piezoelectric coefficient d_{33} = 2820 pC / N and dielectric permittivity $\varepsilon_{33}^{\sigma} / \varepsilon_0$ = 8200 for the PMN–0.33PT SC,[12] we obtain $g_{33} = d_{33} / \varepsilon_{33}^{\sigma}$ = 39.9 mV·m / N. Experimental constants d_{33} = 2890 pC / N and $\varepsilon_{33}^{\sigma} / \varepsilon_0$ = 7700 of the [001]-poled PZN–0.07PT SC[16] lead to g_{33} = 42.4 mV m / N. As is known, the volume-fraction behaviour of the piezoelectric coefficient g_{33}^* in composites[3,11] influences their FOMs to a large extent.

§ The validity of conditions (14) also means that FOMs $(Q_{3j}^*)^2$ from Eq. (11) are characterised by the large anisotropy, *i.e.*, the inequality $(Q_{33}^*)^2 / (Q_{3f}^*)^2 \geq 25$ holds at f = 1 and 2.

1 K. Ren, Y. Liu, X. Geng, H. F. Hofmann, and Q. M. Zhang, *IEEE Trans. Ultrason., Ferroelec., Freq. Contr.*, 2006, **53**, 631.
2 W. Wang, C. He, and Y. Tang, *Mater. Chem. Phys*., 2007, **105**, 273.
3 V. Yu. Topolov, P. Bisegna, and C. R. Bowen, Piezo-active Composites. Orientation Effects and Anisotropy Factors (Springer, Berlin, Heidelberg, 2014).
4 L. Li, S. Zhang, Z. Xu, X. Geng, F. Wen, J. Luo, and T. R. Shrout, *Appl. Phys. Lett*., 2014, **104**, 032909.
5 R. Zhang, B. Jiang, W. Jiang, and W. Cao, *Appl. Phys. Lett*., 2006, **89**, 242908.
6 C. He, W. Jing, F. Wang, K. Zhu, and J. Qiu, *IEEE Trans. Ultrason., Ferroelec., a. Freq. Contr.*, 2011, **58**, 1127.
7 S. Zhang and L. C. Lim, *AIP Advances*, 2018, **8**, 115010.
8 R. E. Newnham, D. P. Skinner, and L. E. Cross, *Mater. Res. Bull.*, 1978, **13**, 525.
9 V. Yu. Topolov, A. V. Krivoruchko, A. N. Isaeva, and A. A. Panich, *Ferroelectrics*, 2020, **567**, 47.
10 J. I. Roscow, H. Pearce, H. Khanbareh, S. Kar-Narayan, and C. R. Bowen, *Eur. Phys. J.: Spec. Top*., 2019, **228**, 1537.
11 V. Yu. Topolov and A. N. Isaeva, *Tech. Phys*., 2021, **66**, 938.
12 R. Zhang, B. Jiang and W. Cao, *J. Appl. Phys*., 2001, **90**, 3471.
13 R. Zhang, W. Jiang, B. Jiang, and W. Cao, in R. E. Cohen (ed.) (2002) Fundamental Physics of Ferroelectrics (American Institute of Physics, Melville), p. 188.
14 G. Liu, W. Jiang, J. Zhu, and W. Cao, *Appl. Phys. Lett.*, 2011, **99,** 162901.
15 J**.** Yin, B. Jiang, and W. Cao, *IEEE Trans. Ultrason. Ferroelectr. Freq. Control*, 2000, **47,** 285**.**
16 R. Zhang, B. Jiang, W, Cao, and A. Amin, *J. Mater. Sci. Lett*., 2002, **21**, 1877.
17 F. Wang, L. Luo, and D. Zhou, *Appl. Phys. Lett***.,** 2007**, 90,** 212903**.**
18 X. Huo, S. Zhang, G. Liu, R, Zhang, J. Luo, R, Sahul, W. Cao, and T.R. Shrout, *J. Appl. Phys*., 2013, **113**, 074106.
19 R. Zhang, B, Jiang, and W. Cao, *Appl. Phys. Lett***.,** 2003**, 82,** 787**.**
20 F. Li, M. J. Cabral, B. Xu, Z. Cheng, E. C. Dickey, J. M. LeBeau, J. Wang, J. Luo, S. Taylor, W. Hackenberger, L. Bellaiche, Z. Xu, L.-Q. Chen, T. R. Shrout, and S. Zhang, *Science*, 2019, **364**, 264.
21 D. La-Orauttapong, B. Noheda, Z.-G. Ye, P. M. Gehring, J. Toulouse, D. E. Cox, and G. Shirane, *Phys. Rev. B*, 2002, **65**, 144101.
22 W. Wang, S. W. Or, Q. Yue, Y. Zhang, J. Jiao, C. M. Leung, X. Zhao, and H. Luo, *Sens. a. Actuators A*, 2013, **196**, 70.
23 A. Safari, M. A. Allahverdi, and E. K. Akdogan, *J. Mater. Sci*., 2006, **41**, 177.
24 A. Safari and E. K. Akdogan, *Ferroelectrics*, 2006, **331**, 153.
25 A. A. Nesterov, V. Yu. Topolov, M. I. Tolstunov, and A. N. Isaeva, *Ceram. Internat*., 2019, **45**, 22241.
26 T. Ikeda, Fundamentals of Piezoelectricity (Oxford University Press, Oxford, New York, Toronto, 1990).
27 M. L. Dunn, *J. Appl. Phys*., 1993, **73**, 5131.
28 J. H. Huang and S. Yu, *Compos. Eng*., 1994, **4**, 1169.
29 F. Levassort, M. Lethiecq, C. Millar, and L. Pourcelot, *IEEE Trans. Ultrason. Ferroelectr. Freq. Control*, 1998, **45**, 1497.
30 I. S. Grigoryev and E. Z. Meylikhov (eds) (1991) Physical Values: Reference Book (Energoatomizdat, Moscow, in Russian).
31 MatWeb: Material property data. www.matweb.com
32 L. V. Gibiansky and S. Torquato, *J. Mech. Phys. Solids*, 1997, **45**, 689.
33 K. E. Evans and K. L. Alderson, *J. Mater. Sci. Lett.*, 1992, **11**, 1721.
34 I. N. Groznov, in Physics Encyclopaedia (Sovetskaya Entsiklopediya, Moscow, 1983, in Russian), p. 178.
35 D. Zhou, K. H. Lam, Y. Chen, Q. Zhang, Y. C. Chiu, H. Luo, J. Dai, and H. L. W. Chan, *Sens. a. Actuators A*, 2012, **182**, 95.
36 H. L. W. Chan and J. Unsworth, *IEEE Trans. Ultrason., Ferroelec., a. Freq. Contr.*, 1989, **36**, 434.
37 V. L. Stuber, D. B. Deutz, J. Bennett, D. Cannel, D. M. de Leeuw, S. van der Zwaag, and P. Groen, *Energy Technol.***,** 2019, **7**, 177.